Available online at www.sciencedirect.com

jmr&t Journal of Materials Research and Technology

www.jmrt.com.br

Original Article

Effect of alkyl chain length of amines on fluorapatite and aluminium phosphates floatabilities

Aline Pereira Leite Nunes[a,*], *Antônio Eduardo Clark Peres*[b], *Arthur Pinto Chaves*[c], *Wanyr Romero Ferreira*[a]

[a] *Faculdade IETEC. Rua Thomé de Souza, 1065, Savassi, CEP: 30140-131 Belo Horizonte, Minas Gerais, Brazil*

[b] *Departamento de Engenharia Metalúrgica e de Materiais, Universidade Federal de Minas Gerais, Escola de Engenharia, Avenida Antônio Carlos, 6627 - Bloco II/2233, CEP: 31270-901 Belo Horizonte, MG, Brazil*

[c] *Escola Politécnica, Universidade de São Paulo. Av. Prof. Mello Moraes, 2373, São Paulo CEP: 05508-900, SP, Brazil*

ARTICLE INFO

Article history:
Received 25 January 2019
Accepted 30 May 2019
Available online 14 June 2019

Keywords:
Fluorapatite
Wavellite
Turquoise
Floatability
Alkyl amine
Zeta potential

ABSTRACT

Microflotation experiments and zeta potential measurements of fluorapatite, wavellite, and turquoise with the use of alkyl amines and amylopectin were conducted. The highest floatability values were achieved in the presence of dodecylamine, exceeding the floatabilities with octylamine between 30% and 90%. Above their respective isoelectric points, the phosphates reached approximately 100% of floatability with dodecylamine. The strong dependence of surfactant adsorption on hydrocarbon chain length was also evidenced by zeta potential results. In the presence of 1×10^{-3} M dodecylamine solution, the surface charge of the phosphates changes from negative to positive until approximately pH 12, while the octylamine was not able to reverse the surface charges. The fluorapatite and wavellite floatabilities were not significantly affected by the amylopectin; however, in the presence of this depressant, the turquoise floatability, with octylamine as collector, decreases abruptly from 93% to 30%. The greater differences observed between turquoise and the other phosphates can be ascribed to their extremely complex structures, chemical composition and its dissolution in aqueous media.

* *Corresponding author at:* TAMIN Engenheiros Associados Ltda. Av. Izabel Bueno, 579, sala 106, Belo Horizonte, Minas Gerais, CEP: 31270-050, Brazil.

E-mails: aline.nunes@taminconsultoria.com.br (A.P. Nunes), aecperes@demet.ufmg.br (A.E. Peres), apchaves@usp.br (A.P. Chaves), diretor.pesquisa@ietec.com.br (W.R. Ferreira).

https://doi.org/10.1016/j.jmrt.2019.05.025

1. Introduction

The processing of low-grade and poor-quality ores with complex mineralogy and resource maximization are two of the several challenges in the mineral processing industry. To improve the performance of numerous flotation systems, the innovation regarding reagents over the last years has been focused on developing reagent-mineral characterization data and extensive structure–property–performance relationships. Therefore, the better selectivity in separation through minimizing the deleterious gangue minerals can be achieved more efficiently and economically via suitable selected reagents [1].

Beneficiation of more than half of the world's marketable phosphate occurs by froth flotation and different reagents are employed in each mineral processing plant. Although the most extensively collectors used in phosphates flotation are long-chain fatty acids and their salts, cationic collectors are employed in the reverse flotation of silicates, dolomitic and calcitic minerals from phosphate minerals. Sodium silicate is more promising as a selective depressant in a wide pH range. However, corn starch has been used widely for increasing selectivity in igneous phosphates flotation, as gangue depressant, for example, in all Brazilian concentrators [2,3].

On other hand, phosphates are undesirable in iron ores, because phosphorus causes negative effects on steel making [4]. In order to reduce the phosphorus content, the reverse flotation with fatty acids as collectors has been widely used for apatite removal from magmatic origin iron ores. However, the phosphorus intensely disseminated as secondary minerals, like wavellite [$Al_3(PO_4)_2(OH)_3{\cdot}5H_2O$] and turquoise [$CuAl_6(PO_4)_4(OH)_8{\cdot}5H_2O$], or adsorbed onto the iron hydroxides render the flotation a challenge [5,6]. Aluminium secondary phosphates, like wavellite and turquoise, are also common in igneous rocks and carbonatitic alkaline complexes and, generally, these phosphates do not affect the beneficiation process. However, their associations with apatite particles decrease the flotation selectivity and, consequently, the total phosphorus recovery [7,8]. Other systems that contain phosphate minerals are some molybdenum oxide ores, where fluorapatite can occur as predominant gangue, jointly with pyrite and quartz. Wang et al. [9] concluded that the flotation separation of molybdenite from fluorapatite could be achieved in weakly alkaline, neutral and acidic pH range with CPC – cetyl pyridinium chloride, a cationic collector type.

The chemical and structural differences among phosphate minerals indicate different results concerning electrokinetic properties and, consequently, froth flotation. Mishra [10] evaluated the floatability of apatites with dodecylamine chloride (DDACl). At the concentration 10^{-4} M, high floatability values, around 100%, were obtained above pH 8 for crystalline fluorapatite, while amorphous fluorapatite did not float. Smani et al. [11] verified floatabilities around 100% between pH 4 and pH 10 when 5×10^{-4} M and 7.5×10^{-4} M solutions of DDACl were used as collector for phosphate oölites from Khouribga, Morocco. In microflotation tests performed by Nunes et al. [6,12], amine based collectors yielded higher values of wavellite floatability than sodium oleate. The authors concluded that since the apatites present higher floatabilities with anionic collectors (fatty acids), the different behaviours between apatite and wavellite could be attributed to the higher stability of the precipitated calcium oleate onto apatite surface compared to the precipitated aluminium oleate onto wavellite surface. Furthermore, the electrostatic interaction between wavellite and amine dissociated species seems to be more intense than in the apatite-amine system.

Since the amine and starch combination has been widely used in several ore flotation concentrators, this work aims to investigate the effect of alkyl chain length of amines on aluminium phosphates and fluorapatite floatabilities, determining the major differences between primary and secondary phosphates. Besides, the objective was also to evaluate the amylopectin as phosphate depressant. The results could expand the understanding of different systems that involve phosphates, mainly as gangue minerals, contributing to the definition of the best selective flotation conditions in several concentrators.

2. Experimental

2.1. Samples preparation and characterization

The wavellite, turquoise and fluorapatite samples, originated from Mauldin Mountain Quarries (USA), Sleeping Beauty Mine (USA), and Ipirá/Pedras Altas (Brazil), respectively, were the same used by Nunes et al. [13], in previous studies.

The phosphate samples were comminuted in a porcelain mortar and the coarser fraction (−300 μm + 75 μm) was used in the microflotation experiments. The finer fraction (−38 μm) was used for the zeta potential measurements.

The samples were qualitatively analysed using an X-ray diffractometer, model PHILIPS PW 1710, CuKα radiation and a graphite monochromator crystal. The results were compared with the standard data base PDF-2 of the ICDD – International Centre for Diffraction Data. The software X'Pert HighScore version 2.1-2004 was used for analysis. SEM/EDS analyses (Scanning Electron Microscope/Energy-Dispersive Spectrometer) were carried out for the coarse fraction (−300 μm + 75 μm). Semiquantitative analyses were performed by X-ray fluorescence in a Philips-Panalytical spectrometer, model PW 2400 with a rhodium anode tube, to check the presence of major constituents and trace elements. Fourier transform infrared spectroscopy analyses (FTIR) were performed with the transmission KBr pellet technique, using a Perkin-Elmer spectrometer, model 1760-X.

2.2. Zeta potential measurements

The zeta potential measurements were performed by the microelectrophoretic technique using the Zeta-Meter System 3.0+ ZM3-D-G with direct video imaging. The zeta potential values were calculated by the Helmholtz-Smoluchowski equation.

Samples of 0.025 g of the mineral of size −38 μm were added into 200 mL of the reagent solution to prepare the suspensions. The suspensions settled during 24 h to produce supernatant particles with a size below 5 μm, according to Stokes's Law; the

Table 1 – Reagents used in the microflotation tests.

Reagent	Chemical formula	Molecular weight (g/mol)
Octylamine	$CH_3—(CH_2)_6—(CH_2)—NH_2$	129.24
Dodecylamine	$CH_3—(CH_2)_{10}-(CH_2)—NH_2$	185.35
Amylopectin	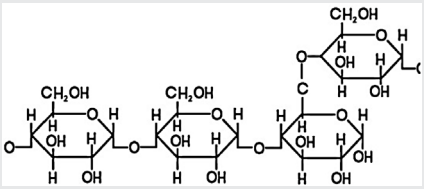	–

sample's specific weights were obtained by helium pycnometry analyses, which were performed using a Quantachrome NOVA 1200.

Sodium nitrate ($NaNO_3$) was used as supporting electrolyte at the concentrations 2.5×10^{-3} M for fluorapatite and 5×10^{-3} M for wavellite and turquoise. The lower concentration in the case of fluorapatite was due to its interaction with sodium nitrate. According to zeta potential results, observed also in previous studies [5,13], the increase in $NaNO_3$ concentration increases the absolute value of fluorapatite zeta potential, indicating that sodium nitrate may not be completely indifferent to this system. The smallest variations of the fluorapatite zeta potential were observed at 2.5×10^{-3} M $NaNO_3$ solution.

The pH values were adjusted with hydrochloric acid (HCl) and sodium hydroxide (NaOH). The measurements were also performed in the presence of surfactants in two concentrations (1×10^{-4} and 1×10^{-3} M) to evaluate the effect of the ions on the phosphate surface characteristics, i.e., on the phosphate electrokinetic behaviour.

2.3. *Microflotation tests*

The microflotation tests were carried out in a modified Hallimond tube at selected pH values varying from 2 to 13. The air flow rate used was 30 mL min^{-1}. The volume of solution in the tube was 180 mL, and the phosphate weight was 1 g for each test. The collector reagents used in the microflotation tests are presented in Table 1. The samples were conditioned with collectors for 5 min and the flotation time in all tests was 3 min. The reagents, all of analytical grade, were prepared at the concentrations 1×10^{-4} and 1×10^{-3} M. Octylamine and dodecylamine were 100% neutralized with acetic acid. The neutralization is an important parameter, since the higher neutralization degrees enhance the collector solubility.

Some tests were also carried out in the presence of amylopectin, under alkaline pH, to check the depressant effect of this reagent on the phosphates floatability. In these tests, the collectors were used at the concentration 1×10^{-4} M. The amylopectin solubilization was achieved by adding sodium hydroxide at the weight ratio 5:1. The mineral samples were

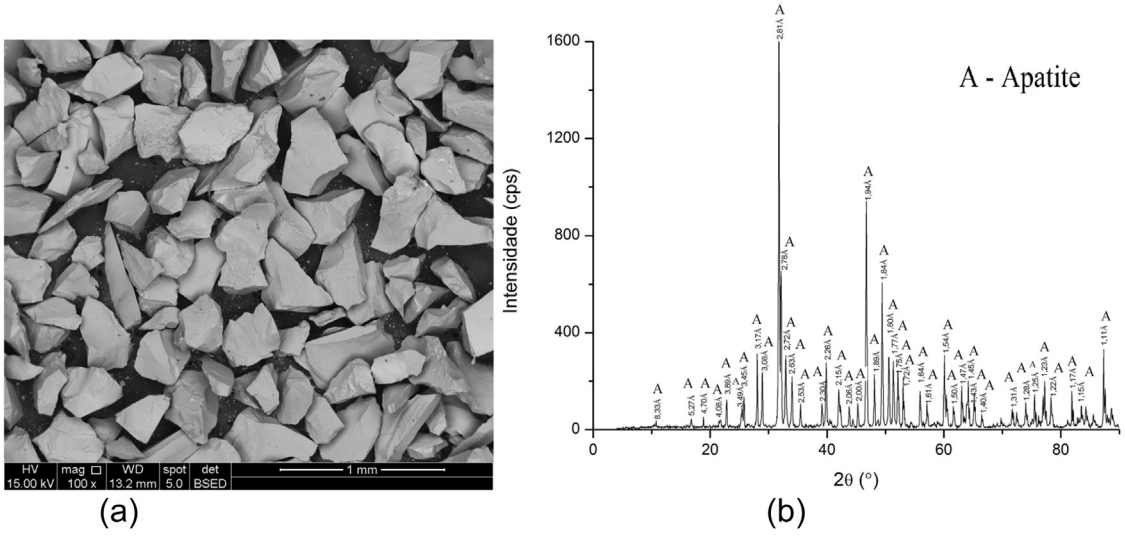

Fig. 1 – (a) SEM, backscattered electron images (BSE) and (b) XRD pattern for apatite sample.

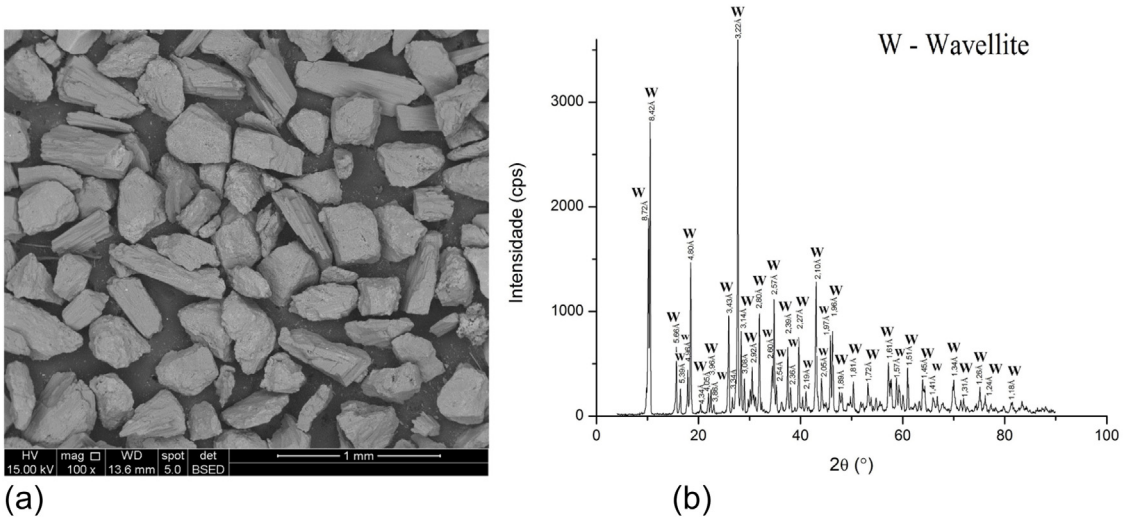

Fig. 2 – (a) SEM, backscattered electron images (BSE) and (b) XRD pattern for wavellite sample.

conditioned in a 90 mL volume of amylopectin solution, at the concentrations 5, 10, 20, 40 and 80 mg L^{-1}, for 5 min. Immediately, 90 mL of collector solution 2×10^{-4} M (resulting in 1×10^{-4} M final concentration) were added. The collector conditioning time was 5 min and the flotation time was 3 min.

3. Results and discussion

3.1. *Samples characterization*

The samples were analysed by SEM/EDS and the habit of the crystals by backscattered electrons image (BSE) were observed (Figs. 1–3). The apatite and wavellite crystals showed good crystallization, however, turquoise crystals seem to be more massive and earthy. The SEM/EDS and X-ray diffraction results corroborated the samples' high purity because no other phases were detected in each diffractogram, as can be seen in Figs. 1–3. Concerning the fluorapatite and wavellite (Figs. 1(b) and 2(b)), amorphization domes were not observed, indicating the absence of amorphous phases. However, in the XRD pattern of turquoise (Fig. 3(b)), amorphization tendency was observed, indicating lower crystallization degree than fluorapatite and wavellite samples.

As reported by Nunes et al. [13], the XRF analyses confirming the phosphate samples purity, and the detection of fluoride in the fluorapatite sample indicated that this element is likely present in the sample at concentrations above the detection limit, thus confirming that the apatite sample consists mainly of fluorapatite. In the FTIR spectrum obtained for the fluorapatite (Fig. 4), the displacement of the OH vibration band to 3525 cm^{-1} and 742 cm^{-1}, characteristic of the interactions between OH groups and fluorine [14], and the presence of CO_3^{2-} stretching vibration at 1424–1461 cm^{-1} further confirms that the sample is a fluor-hydroxi-carbonate-apatite. As reported by Araujo [15], the position of CO_3^{2-} stretching vibration indicates that this sample is a carbonate-apatite characterized by CO_3^{2-} groups replacing in part the PO_4^{3-}

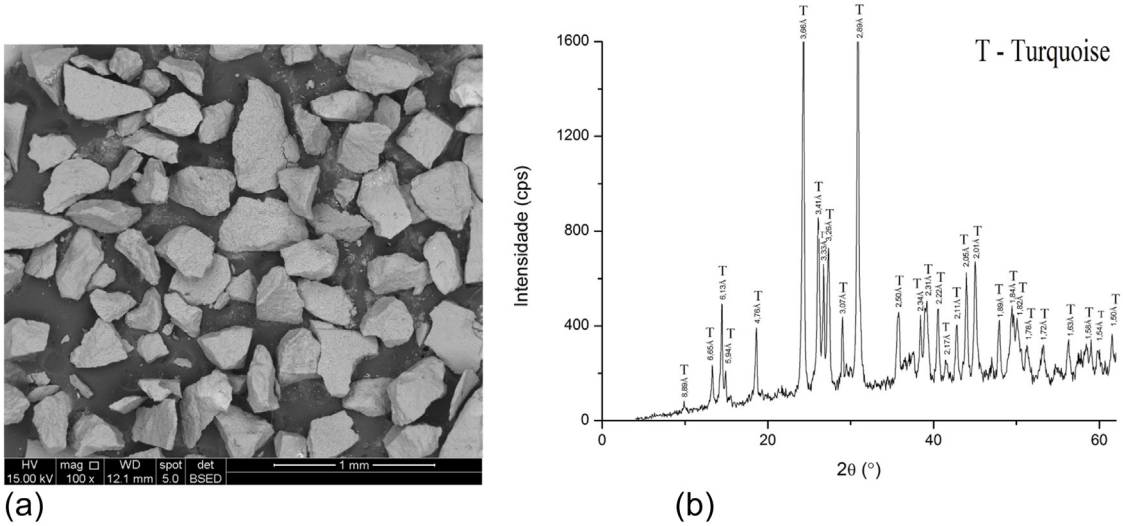

Fig. 3 – (a) SEM, backscattered electron images (BSE) and (b) XRD pattern for turquoise sample.

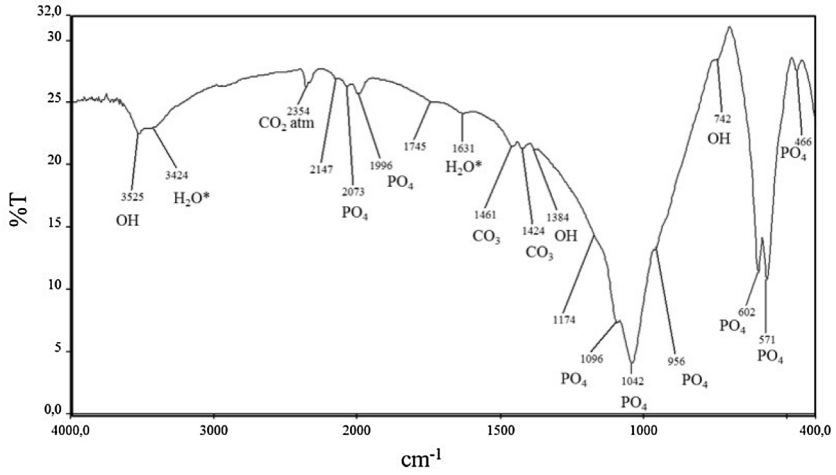

Fig. 4 – FTIR spectrum for apatite sample.

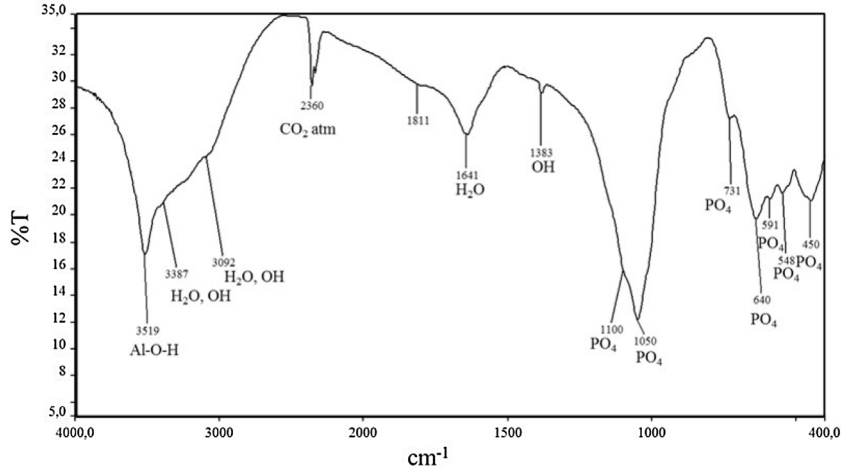

Fig. 5 – FTIR spectrum for wavellite sample.

groups. According to the author, other carbonate-apatite types present CO_3^{2-} groups inside "tunnels" of the crystal lattice, exhibiting stretching vibration at 1465–1542 cm^{-1}. Besides these two vibrational modes, and 860–885 cm^{-1} in and out bending mode, other carbonate vibrational modes are generally absent in the infrared spectra of carbonate-apatites [15].

The symmetric and antisymmetric stretching vibrations of the PO_4^{3-} groups were observed in all FTIR spectra, mainly at 900 cm^{-1} and 1100 cm^{-1} (Figs. 4–6).

In the FTIR spectrum for wavellite sample (Fig. 5), the stretching vibration bands related to the PO_4^{3-} groups were observed at 1050–1100 cm^{-1}, while in the turquoise spectrum (Fig. 6) these bands are observed in the 1012–1192 cm^{-1} region. The phosphate deformation modes are identified below 731 cm^{-1} in the wavellite spectrum and 724 cm^{-1} in the turquoise spectrum. The bending vibrations of the water molecules of the wavellite and turquoise can be observed at 1641 cm^{-1} and 1631 cm^{-1}, respectively. The strong bands in the wavellite and turquoise spectra at 3519 cm^{-1} and 3510 cm^{-1}, respectively, can be ascribed to the stretching vibrations of the oxygen and hydrogen bonds related to the Al—O—H groups in aluminium phosphates. In the FTIR spectrum of turquoise, the vibration bands at 611 cm^{-1} can be ascribed to the copper–oxygen bonds.

3.2. *Fluorapatite floatability*

The results of fluorapatite floatability and zeta potential measurements in the presence of octylamine and dodecylamine acetates are presented in Fig. 7. The maximum floatability, in the 1×10^{-4} M octylamine solution, was 62.2%, achieved at pH 11. In the 1×10^{-3} M solution, two maxima values (above 90%) occur at approximately pH 6.5 and pH 10.5.

The dodecylamine is a more effective collector for fluorapatite than octylamine, as can be seen in Fig. 7(b). The floatability was approximately 100% in all investigated pH range, showing the strong dependence of the surfactant adsorption on chain length. Besides, the zeta potential is reverted from negative to positive between pH 6 and pH 8.5 at 1×10^{-4} M solution and until approximately pH 12 at 1×10^{-3} M solution.

The predominant species for amines in the acidic and neutral pH regions are the cationic species (RNH_3^+ and $(RNH_3)_2^{2+}$),

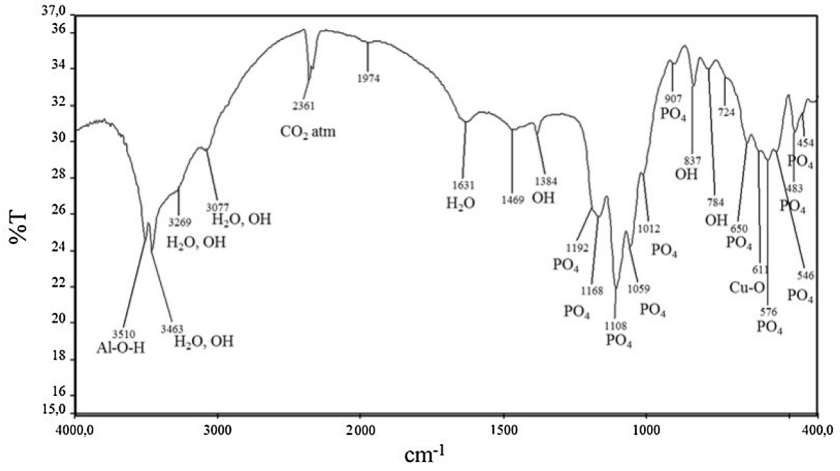

Fig. 6 – FTIR spectrum for turquoise sample.

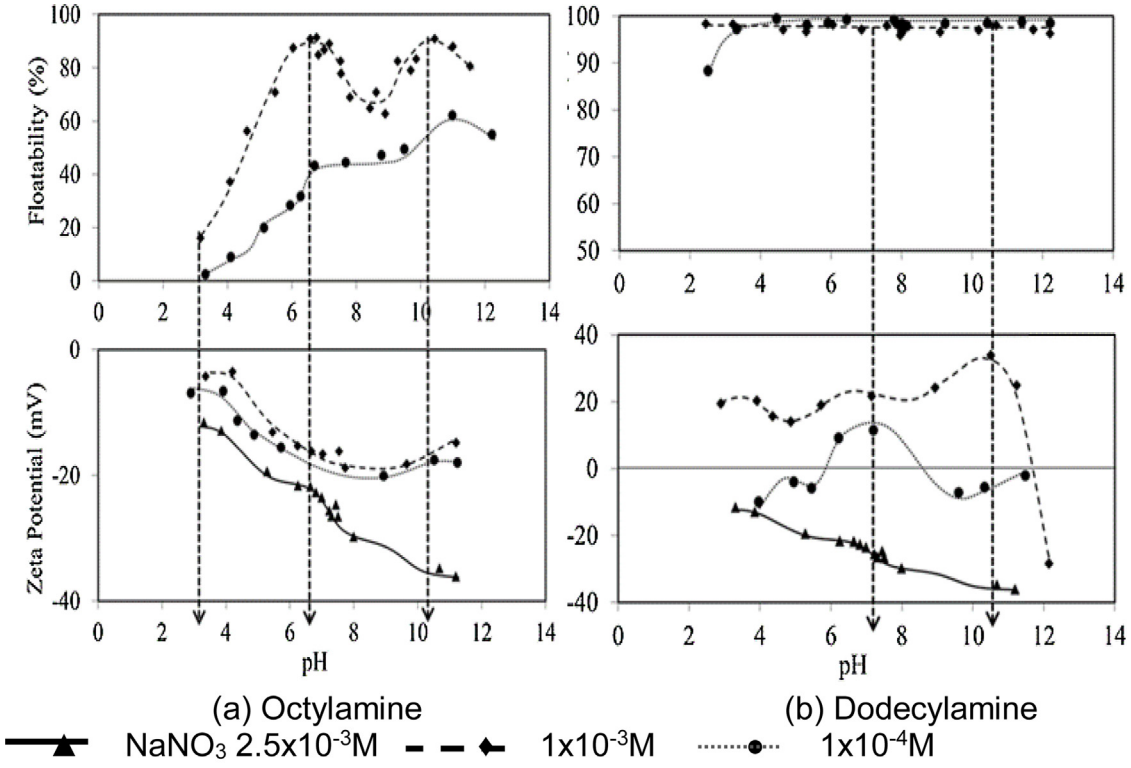

Fig. 7 – Microflotation curves and zeta potential for fluorapatite sample with octylamine (a) and dodecylamine (b).

and the neutral molecules ($RNH_{2(aq)}$) precipitates in the alkaline pH range. The continuous rise in the floatability until pH 6.5 observed in Fig. 7(a) suggests octylamine adsorption due to the electrostatic interactions between negative surface sites and dissociated amine species. However, jointly electrostatic interactions, hydrogen bonds between negative surface sites, mainly sites that contain fluorine, and amine dissociated species, must be considered (Fig. 8(a) and (b)). Until pH 6.5, these interactions can be described by the reaction:

$$\equiv OHF^{-} + RNH_3^{+} \leftrightarrow \equiv OHF^{-}\ldots{}^{+}H_3NR \quad (1)$$

Amines can also undergo additional intramolecular reactions in aqueous media, forming ionomolecular complexes ($(RNH_2RNH_3)^{+}$) by association of aminium ion and neutral amine molecule and dimerization of aminium ions ($(RNH_3)_2^{2+}$). The ionomolecular complexes present high activity between pH 9 and pH 11, while the dimers are highly active between pH 6 and pH 10.5 [16]. The high activities of the dimeric species between approximately pH 6 and pH 10 may justify the floatability decrease in this region (Fig. 7). These dimeric species certainly participate of the adsorption onto apatite, rendering the surface less hydrophobic due the charge excess generated after the adsorption, related to the polar head groups projected outwards. Normal bonds, responsible

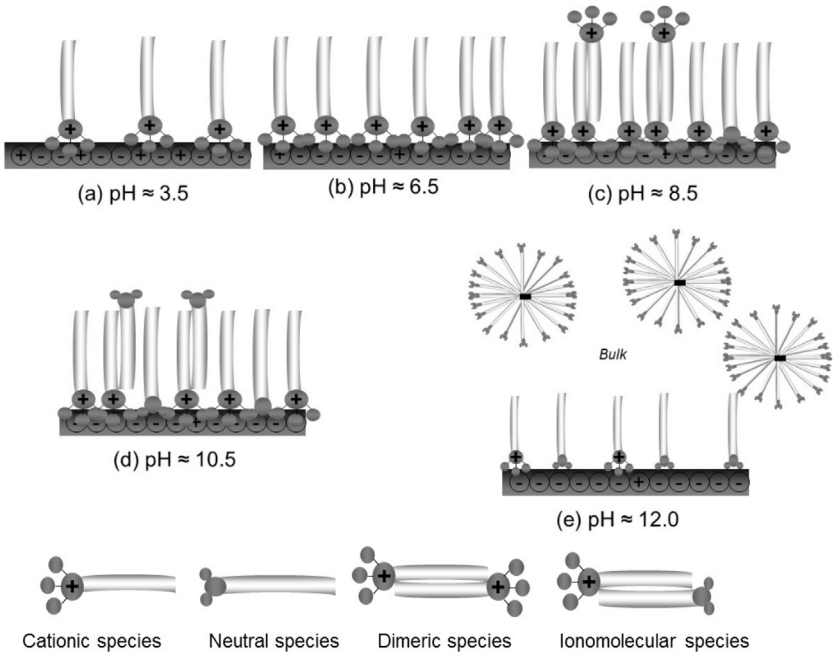

Fig. 8 – Proposed scheme for interaction mechanisms between octylamine and fluorapatite surface, at different pH ranges.

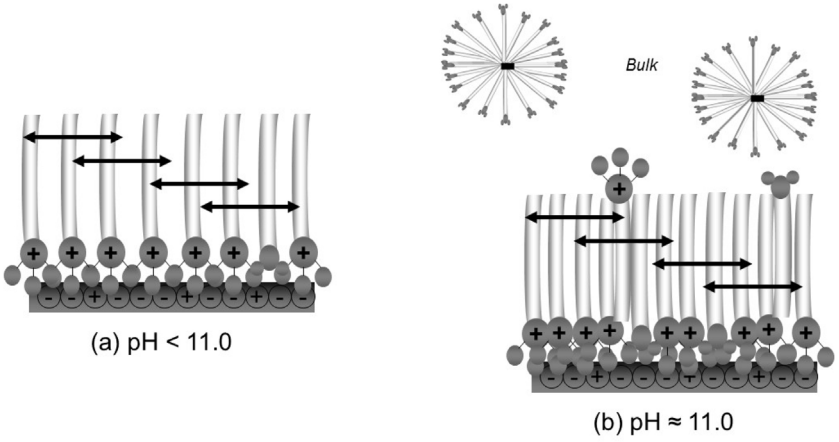

Fig. 9 – Proposed scheme for interaction mechanisms between dodecylamine and fluorapatite surface, at different pH ranges.

for adsorption, force the surfactant to adsorb on the solid with the other polar head groups fixed at the solid (Fig. 8(c)):

$$\overline{\equiv}OHF^- + (RNH_3)_2^{2+} \leftrightarrow \overline{\equiv}OHF^- \ldots^+(H_3NR)(H_3NR)^+ \quad (2)$$

Above pH 9, the ionomolecular species of the octylamine become predominant and restore the fluorapatite floatability through hydrogen bonds between fluorapatite and ionomolecular species (Fig. 8(d)):

$$\overline{\equiv}OHF^- + (RNH_2RNH_3)^+ \leftrightarrow \overline{\equiv}OHF^- \ldots^+(H_3NR..RNH_2) \quad (3)$$

Adsorption of dodecylamine onto fluorapatite can also be described by reactions (1)–(3), and the fluorapatite floatabilities indicate the high influence of the hydrocarbon chain length, corroborating previous studies addressing the effects of surfactant chain length on adsorption. Increasing the hydrocarbon chain length, the aversion between the surfactant molecules and aqueous medium becomes more intense, due the hydrophobicity increase imparted by the surfactants' longer tail, increasing the aggregation tendency [17–21]. Considering molecular association into two-dimensional aggregates [22] normal bonds are responsible for polar head–surface interactions and hydrophobic interactions will occur laterally between the hydrocarbon chains of the adsorbed surfactant, providing the attractive force to promote two-dimensional condensation as well as the formation of patches. Therefore, the longer chain will promote enhancement of the adsorption onto mineral surface, since the chain–chain hydrophobic interaction will be sufficiently strong to anchor more surfactant molecules onto mineral surface, leading to the compact hemimicelle formation, even at

low concentrations. The excessive dodecylamine adsorption onto fluorapatite causing the increase in the zeta potential, as can be seen in Fig. 7(b), while even at 1×10^{-3} M, the octylamine did not reverse the surface charge (Fig. 7(a)), can be explained by these phenomena (Fig. 9(a) and (b)).

Considering the occurrence of amine species precipitation, the fluorapatite floatability above pH 9 shown in Fig. 7(a) may also be attributed to amine colloids precipitated onto fluorapatite surface, as additional adsorption mechanism. The increase in the zeta potential values, above pH 9 at the 1×10^{-3} M and pH 9.5 at the 1×10^{-4} M, makes this hypothesis reasonable, once these pH values are coincident with the critical pH of amine precipitation [23]. In addition, the pre-precipitation of the ionomolecular species onto the surface would cause the decrease in the floatability at pH 9 and the redispersion would be responsible for the new increase in the floatability until pH 10.8 [16]. The decrease in the floatability above pH 11 can be due to the negative charge of the amine colloids (Fig. 8(e)), which present PZC at pH 11 [24].

The fluorapatite floatability was not significantly affected by the presence of amylopectin even at high concentrations, as can be seen in Fig. 10. Sterical hindrance effects may be considered as a hypothesis for these results, being explained by the position of the hydroxyl groups in amylopectin not fitting the spacing between the fluorapatite surface active sites. In fact, Leal Filho et al. [25] ascribed the starch and ethyl-cellulose inabilities to depress hydroxyapatite to sterical hindrance effects, since they obtained low values of fitting number (a measure of the steric compatibility) for the interaction apatite/starch and apatite/ethyl-cellulose through modelling mineral surfaces and polysaccharides molecules.

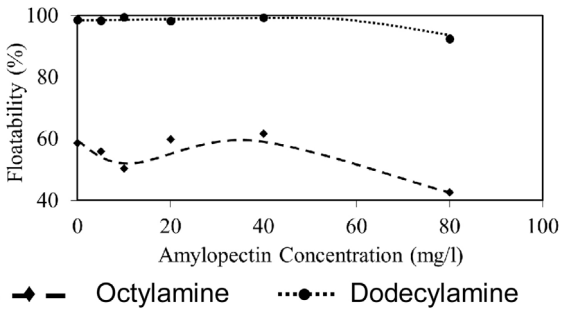

Fig. 10 – Microflotation curves for fluorapatite sample with collectors and amylopectin at pH 10.5. Collector concentrations: 1×10^{-4} M.

Another hypothesis to explain the low depressant effect is the fact that the collector dosage is sufficient to prevent amylopectin adsorption onto the mineral.

Araujo [15] investigated also the fluorapatite floatability in the presence of starch, amylose and amylopectin. The three compounds effectively depressed the fluorapatite. Pinto et al. [26] also obtained expressive depressant effects of the starch onto apatite. However, Mohammadkhani et al. [27], evaluating the selective conditions to recover phosphate from a very low-grade sedimentary ore through reverse flotation, observed that starch was ineffective to depress the phosphates. Therefore, different results related to the starch's depressant action on apatite can be ascribed to extremely complex crystal structures, besides ion replacements and its dissolution in aqueous media. These properties lead to high dependency of adsorp-

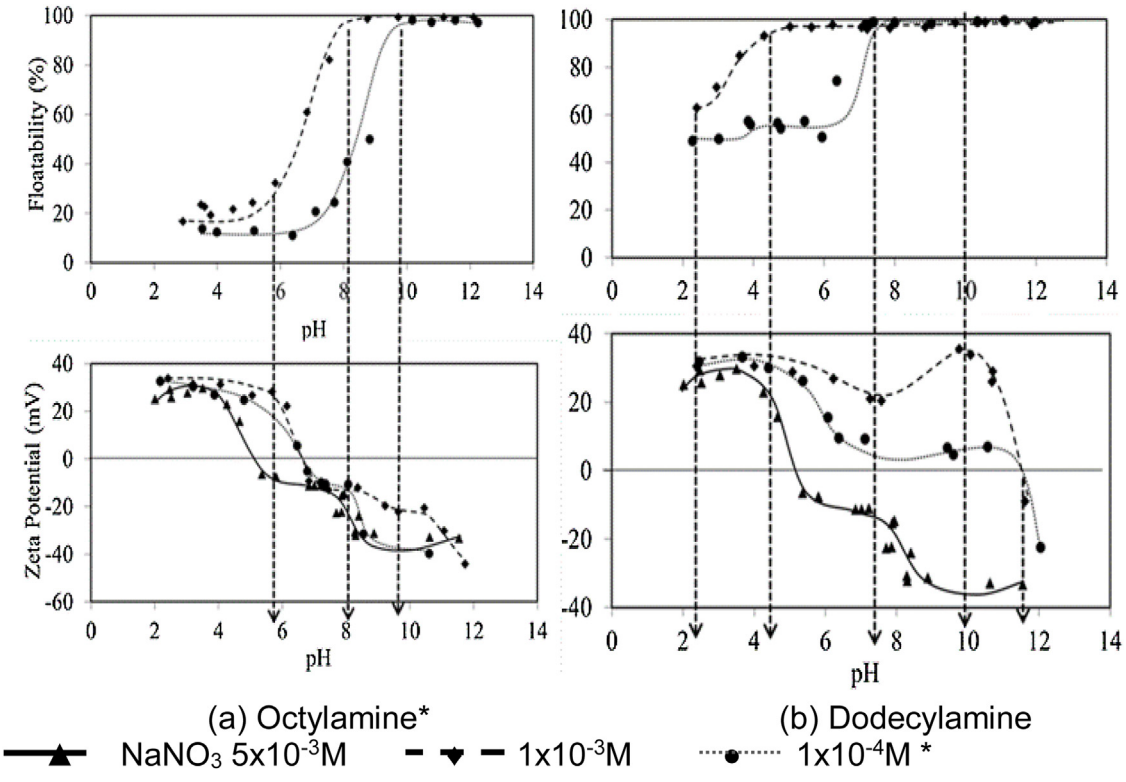

Fig. 11 – Microflotation curves and zeta potential for wavellite sample with octylamine (a) and dodecylamine (b). *According to Nunes et al. [12].

tion mechanism on the mineral specificity, genesis, and its surface properties [28–33].

3.3. *Floatability of wavellite*

The secondary phosphates have higher chemical and structural complexities than apatite [12,13]. Therefore, this mineral class will present major differences regarding interfacial properties and, consequently, in flotation results. Confirming this perspective, great differences between the apatite and wavellite floatabilities with octylamine and dodecylamine were detected, as can be seen in Fig. 11.

Below pH 5.2, where the IEP of wavellite occurs [13], the low floatabilities support the hypothesis that interactions of chemical nature concur with electrostatic repulsion, and the latter is predominant. As the pH increases, the wavellite becomes progressively more negative, favouring the electrostatic interaction with surfactant and, consequently, the hemimicelle formation. Therefore, between pH 6 and 10, for both concentrations, the abrupt rise in floatability could be ascribed to the hemimicelle formation. The wavellite floatabilities with octylamine achieved values close to 100% above pH 8 at the 1×10^{-3} M concentration, and above pH 10 at the 1×10^{-4} M concentration.

The octylamine renders the wavellite surface less negatively charged and shifts the IEP from pH 5.2 to approximately pH 6.5 at the both concentrations. The onset of hemimicelle formation at 1×10^{-3} M coincides with the IEP, at pH 5.2, which indicates electrostatic attraction. At the 1×10^{-4} M concentration, the same mechanism is considered, since the onset occurs where the surface and collector are oppositely charged. The higher floatabilities occur when the wavellite is more negatively charged.

According to Nunes et al. [12], the adsorption of amines onto wavellite can be attributed to both chemical and electrostatic interactions. This hypothesis would be explained by wavellite floatability with dodecylamine, as can be seen in Fig. 11(b). Below the IEP, where wavellite was more positively charged, a rapid rise in floatability is observed at 1×10^{-3} M; the values achieved 100% near pH 5. Nunes et al. [12] proposed also the adsorption of amines onto wavellite by hydrogen bonds between neutral surface sites and amine dissociated species. According to these authors, the mineral surface becomes more positively charged due this adsorption, which can be described by the reactions:

$$\equiv\overline{\mathrm{AlOH}} + \mathrm{RNH_3}^{+} \leftrightarrow \equiv\overline{\mathrm{AlOH_2}}\ldots{}^{+}\mathrm{NH_2R} \quad (4)$$

$$\equiv\overline{\mathrm{AlOH}} + (\mathrm{RNH_2RNH_3})^{+} \leftrightarrow \equiv\overline{\mathrm{AlOH_2}}\ldots{}^{+}(\mathrm{NH_2R})_2 \quad (5)$$

$$\equiv\overline{\mathrm{AlOH}} + (\mathrm{RNH_3})_2{}^{2+} \leftrightarrow \equiv\overline{\mathrm{AlOH_2}}\ldots{}^{+}(\mathrm{NH_2R})^{+}(\mathrm{NH_3R}) \quad (6)$$

These interactions can also explain the high wavellite floatabilities with dodecylamine below its IEP, justifying also the more positively charged surface in the surfactant presence. Until pH 10.6, the high wavellite floatabilities with both octylamine and dodecylamine are the result of interactions between amine dissociated species and active sites at the wavellite surface. Above this pH, the floatability could be explained by the precipitation of amine colloids onto the wavellite surface. As in fluorapatite, the zeta potential curves reinforce this hypothesis, once the pH range of the high zeta potential values are coincident with the critical pH of precipitation and PZC of the amine colloids at pH 11 [24].

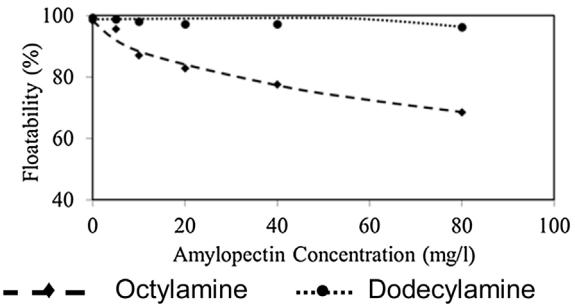

Fig. 12 – Microflotation curves for wavellite sample with collectors and amylopectin at pH 10.5. Collector concentrations: 1×10^{-4} M.

The onset of rise in the floatability at 1×10^{-4} M, for both octylamine and dodecylamine, occurs only at pH 7.0, where the surface becomes more negatively charged, evidencing the strong role of the electrostatic mechanisms. Reinforcing this hypothesis, the dodecylamine reverses the wavellite surface charge until pH 11.5.

As the fluorapatite, the wavellite floatability was not significantly affected by the presence of amylopectin. These results, presented in Fig. 12, were similar to those reported previously by Nunes et al. [12], achieved in the presence of corn starch. Although the floatability with octylamine decreases from 100% in the absence of amylopectin to 70% in the presence of 80 mg/L amylopectin solution, no depressant action was observed using dodecylamine as collector.

Two hypotheses were proposed to explain the low depressant effect of starch onto wavellite [12]. The first refers to the amount of complexes formed through the starch hydroxyl groups and Al cations (Al^{3+}, $Al(OH)_2{}^{+}$, e $Al(OH)^{2+}$) onto the mineral surface; the drop in Al cations concentrations in the wavellite surface active sites prevents the formation of complexes with the starch, inhibiting the adsorption. The other one is related to the sterical hindrance effects, as the position of hydroxyl groups in starch may not fit the spacing between wavellite surface active sites.

3.4. *Floatability of turquoise*

As fluorapatite, the turquoise presented lower floatability with octylamine than wavellite (Fig. 13(a)). Between pH 3 and pH 6, the floatability is negligible at the concentration 1×10^{-4} M. However, the floatability values achieve more than 40% at the concentration 1×10^{-3} M, in the same pH region, and the maximum of 100% is achieved above pH 9.

Considering the electrokinetic properties of turquoise and its floatabilities presented in Fig. 13, the electrostatic adsorption seems to be the main mechanism for interaction between amines and turquoise above the IEP, which occurs at pH 7.2 [13]. The floatabilities increase sharply above the IEP, where the mineral surface becomes negatively charged.

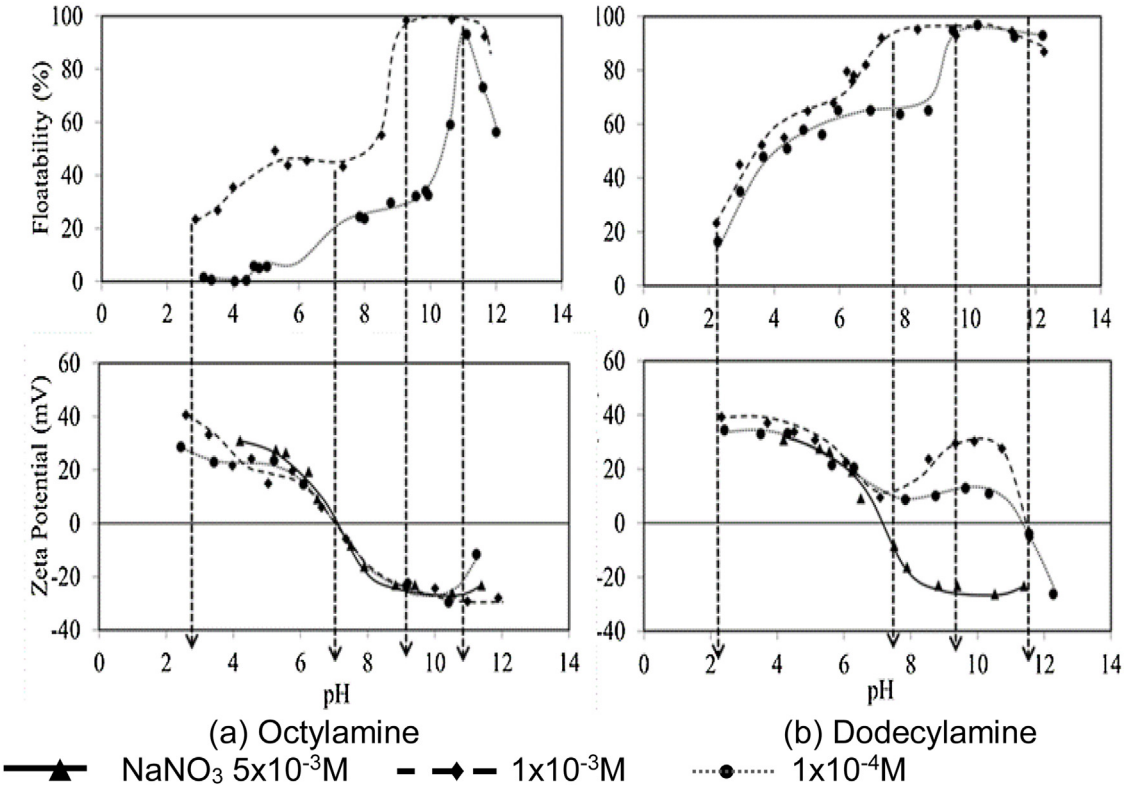

Fig. 13 – Microflotation curves and zeta potential for turquoise sample with octylamine (a) and dodecylamine (b).

Below the IEP both mineral surface and collector charges are positive. So, chemical adsorption mechanism must be necessary to yield floatability levels above 40% for the octylamine concentration 1×10^{-3} M. Considering that both chemical adsorption and electrostatic repulsion are present, one hypothesis is proposed: small amounts of amine dissociated species are required by turquoise to become slightly hydrophobic. The results are the relative floatability and zeta potential magnitude maintenance, relative to the mineral surface in the absence of collector.

As already proposed for the wavellite-octylamine system, the turquoise floatability can be due to the adsorption of amine dissociated species onto neutral surface sites, through hydrogen bonds. Therefore, besides Eqs. (4)–(6) where amine species adsorb onto neutral sites containing aluminium, other analogue reactions for octylamine adsorption onto neutral surface sites containing copper are proposed:

$$\equiv CuOH + RNH_3^+ \leftrightarrow \equiv CuOH_2 \ldots {}^+NH_2R \quad (7)$$

$$\equiv CuOH + (RNH_2RNH_3)^+ \leftrightarrow \equiv CuOH_2 \ldots {}^+(NH_2R)_2 \quad (8)$$

$$\equiv CuOH + (RNH_3)_2{}^{2+} \leftrightarrow \equiv CuOH_2 \ldots {}^+(NH_2R)^+(NH_3R) \quad (9)$$

Until pH 7, the lower floatability values could be attributed, partially, to a higher surface active cations number than in the case of both fluorapatite and wavellite, i.e., the turquoise has in its structure two elements, copper and aluminium, that contribute with positive charges. Therefore, the chemical adsorption concurs with electrostatic repulsion, and the latter is predominant.

Another notable aspect observed in Fig. 13(b) is the unaltered zeta potential for both concentrations of dodecylamine, until the IEP. Additionally, between pH 2 and pH 9, the floatability increases gradually at the 1×10^{-4} M concentration. Above pH 9, the interaction between collector and mineral surface causes the rapid rise in floatability. At the 1×10^{-3} M concentration, this increase is observed above pH 6. The zeta potential is reversed above the IEP in the presence of dodecylamine, achieving high positive values joint to high floatability values, indicating the hemimicelle formation. Therefore, it can be concluded that the electrostatic mechanism becomes essential.

Until pH 9, the turquoise floatabilities with dodecylamine are result of interactions between amine dissociated species and active sites at the turquoise surface, probably by electrostatic and chemical interactions. Above this pH value, the floatability values near 100% could also be explained by precipitation of amine colloids onto the mineral surface. The zeta potential curves in Fig. 13(b) show the continuous increase where the critical pH of precipitation and the PZC of the amine colloids occur. Above pH 11, where the PZC of the amine occurs, the floatability decreases abruptly, as a result of the sign reversal of the precipitated colloid surface charge.

In Fig. 14 are presented the results of turquoise floatability in the presence of amylopectin. The floatability with octylamine decreases from 93% in the absence of amylopectin, to 30% in the concentration 80 mg/L. The same behaviour was

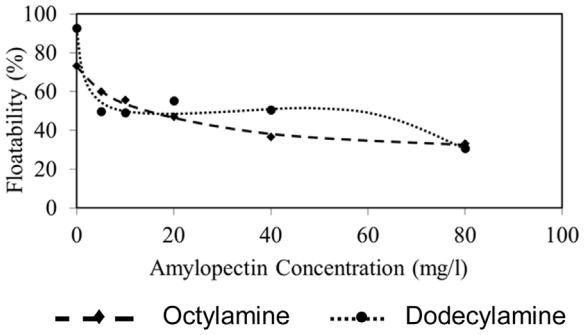

Fig. 14 – Microflotation curves for turquoise sample with collectors and amylopectin at pH 11. Collector concentrations: 1×10^{-4} M.

observed for dodecylamine, where the floatability decreases from 83% to 30%.

One hypothesis for the depressant effect of amylopectin onto turquoise is the formation of complexes through the amylopectin hydroxyl groups and Cu and Al cations (Cu^{2+}, Al^{3+}, $Al(OH)_2^+$, and $Al(OH)^{2+}$), on the mineral surface, favouring the depression. As reported by Nunes et al. [13], turquoise has two elements that contribute to positive charges in its structure, as potential determining ions – PDI, namely, copper and aluminium. Wavellite has only aluminium as its cationic PDI. Besides, the apatite, composed mainly of fluorapatite, presented a negative surface charge in the full pH range evaluated, and has only species Ca^{2+} as cationic PDI [13]. Therefore, the amount of the cationic species in phosphate crystal structures seems to be a considerable explanation to the different results in presence of amylopectin obtained for the fluorapatite, wavellite, and turquoise: higher cation amounts lead to higher starch adsorption, improving the depressant effect.

This hypothesis can be reinforced by the effects of cation concentrations on the selective flocculation of different ores using starch [34–36]. Using natural iron ores in a pilot-scale desliming thickener, Haselhuhnt and Kawatra [35] verified that increases in the calcium concentration within the process water resulted in higher metallurgical recoveries. Eisele et al. [37] verified that in the filter cake of the magnetite concentrate, the calcium concentrations were 565 times higher than in the filtrate water. These results indicate the strong starch adsortpion induced by cations amounts present in the systems, improving the aggregation processes.

4. Conclusions

The fluorapatite floatability in the 1×10^{-4} M octylamine solution presented low values. The floatability values with dodecylamine can exceed between 30% and 90% the floatabilities with octylamine. Besides, while in the octylamine solutions the fluorapatite charge remains negative, with dodecylamine the zeta potential changes sign from negative to positive until approximately pH 12, evidencing the strong dependence of the surfactant adsorption on chain length. The fluorapatite floatability was not significantly affected by the presence of amylopectin.

The high wavellite floatabilities with dodecylamine below its IEP can be ascribed to hydrogen bonds between neutral surface sites of wavellite and amine dissociated species. However, the onset of rise in the floatability at the 1×10^{-4} M occurs only pH 7.0, where the surface becomes more negatively charged, evidencing the strong role of the electrostatic mechanisms. Besides, the dodecylamine reverses the wavellite surface charge until pH 11.5, evidencing a hydrophobic surface after longer hydrocarbon chain adsorption. The amylopectin presented moderate depressant effect on wavellite in the presence of octylamine. However, this reagent was completely ineffective using dodecylamine as collector.

As already proposed for the wavellite-octylamine system, the turquoise floatability can also be due to the adsorption, via hydrogen bonds, of amine dissociated species onto neutral sites containing aluminium and copper. Above the IEP, the zeta potential is reversed, achieving high positive values jointly the high floatability values, indicating hemimicelle formation and the dependence of floatability on hydrocarbon chain length. The turquoise floatability decreases from 93% in the absence of amylopectin, to 30% in the concentration 80 mg/L, using octylamine. For dodecylamine, the floatability decreases from 83% to 30%. Therefore, the amount of the cationic species in phosphate crystal structures seems to be an explanation for the results in the presence of amylopectin. The higher cation amounts lead to higher starch adsorption, improving the depressant effect.

Conflicts of interest

The authors declare no conflicts of interest.

Acknowledgments

This study was financed in part by the Coordenação de Aperfeiçoamento de Pessoal de Nível Superior – Brasil (CAPES) – Finance Code 001, CNPq and FAPEMIG.

REFERENCES

[1] Nagaraj DR, Farinato RS. Evolution of flotation chemistry and chemicals: a century of innovations and the lingering challenges. Min Eng 2016;96–97:2.
[2] Guimarães RC, Araujo AC, Peres AEC. Reagents in igneous phosphate ores flotation. Min Eng 2005;199–204:18.
[3] Sis H, Chander S. Adsorption and contact angle of single and binary mixtures of surfactants on apatite. Min Eng 2003;16:839.
[4] Chiaverini V. Aços e ferros fundidos: características gerais, tratamentos térmicos, principais tipos. 7ª edição São Paulo: ABM; 2008. p. 177.
[5] Nunes APL. Doctoral thesis, Estudos Eletrocinéticos e Flotabilidade da Wavellita, Turquesa, Senegalita e Apatita. Belo Horizonte: Escola de Engenharia da UFMG; 2012. p. 223 (in Portuguese).
[6] Nunes APL, Pinto CLL, Valadão GES, Viana PRM. Floatability studies of wavellite and preliminary results on phosphorus removal from a Brazilian iron ore by froth flotation. Min Eng 2012;39:206.

[7] Kahn H, SanÍAgostino LM, Tassinari MMML, Ulsen C, Braz AB. Apatite from alkaline complexes: behavior in mineral processing and characterization techniques. In: Zhang P, Swager K, Leal Filho L, El-Shall H, editors. Beneficiation of phosphates: technology advance and adoption. Littleton: SME; 2010. p. 53.
[8] Toledo MCM. Os fosfatos aluminosos da série da crandallita uma revisão. Rev Inst Geológico 1999;20:49.
[9] Wang Z, Xu L, Liu R, Sun W, Xiao J. Comparative studies of flotation and adsorption with cetyl pyridinium chloride on molybdite and fluorapatite. Int J Miner Process 2015;143:112.
[10] Mishra SK. The electrokinetic properties and flotation behaviour of apatite and calcite in the presence of dodecylamine chloride. Int J Miner Process 1979;6:119.
[11] Smani MS, Blazy P, Cases JM. Beneficiation of sedimentary moroccan phosphate ores; part III: selective flotation and recovery. Trans SME/AIME 1975;258:176.
[12] Nunes APL, Peres AEC, Araujo AC, Valadão GES. Electrokinetic properties of wavellite and its floatability with cationic and anionic collectors. J Colloid Interface Sci 2011;361:632.
[13] Nunes APL, Peres AEC, Valadão GES. The influence of lattice ions on the electrokinetic potential of primary and secondary phosphates. Sep Sci Technol 2015;50:2023.
[14] Ross SD. Phosphates and others oxy-anions of group V. In: Farmer VC, editor. The infrared spectra of minerals. London: Mineralogical Society; 1974. p. 383.
[15] Araujo AC. PhD Thesis, Starch modification of the flocculation and flotation of apatite. University of British Columbia; 1988. p. 379.
[16] Finch JA, Smith GW. Dynamic surface tension of alkaline dodecylamine solutions. J Colloid Interface Sci 1973;45:81.
[17] Paria S, Khilar KC. A review on experimental studies of surfactant adsorption at the hydrophilic solid–water interface. Adv Colloid Interface Sci 2004;110:75.
[18] Atkin R, Craig VSJ, Wanless EJ, Biggs SJ. The influence of chain length and electrolyte on the adsorption kinetics of cationic surfactants at the silica–aqueous solution interface. Colloid Interface Sci 2003;266:236.
[19] Wu SH, Pendleton P. Adsorption of anionic surfactant by activated carbon: effect of surface chemistry, ionic strength, and hydrophobicity. J Colloid Interface Sci 2001;243:306.
[20] Wang W, Kwak JCT. Adsorption at the alumina–water interface from mixed surfactant solutions. Colloids Surf A 1999;156:95.
[21] Somasundaran P, Healy TW, Fuerstenau DW. Surfactant adsorption at solid–liquid interface-dependence of mechanism on chain length. J Phys Chem 1964;68:3562.
[22] Cases JM, Villieras F. Thermodynamic model of ionic and nonionic surfactant adsorption–abstraction on heterogeneous surfaces. Langmuir 1992;8:1251.
[23] Laskowski JS, Vurdela RM, Liu Q. The colloid chemistry of weak-electrolyte collector flotation. In: Forrsberg KSE, editor. Development in mineral processing. Proceedings of the XVI Int. Miner. Processing Congress. Amsterdan: Elsevier; 1988. p. 703.
[24] Castro SH, Vurdela RM, Laskowski JS. The surface association and precipitation of surfactant species in alkaline dodecylamine hydrochloride solutions. Colloids Surf 1986;21:87.
[25] Leal Filho LS, Seidl PR, Correia JCG, Cerqueira LCK. Molecular modelling of reagents for flotation processes. Min Eng 2000;13:1495.
[26] Pinto CLL, Araujo AC, Peres AEC. The effect of starch, amylose and amylopectin on the depression of oxi-minerals. Min Eng 1992;5:469.
[27] Mohammadkhani M, Noaparast M, Shafaei SZ, Amini A, Amini E, Abdollahi H. Double reverse flotation of a very low grade sedimentary phosphate rock, rich in carbonate and silicate. Int J Miner Process 2011;100:157.
[28] Skartsila K, Spanos NJ. Surface characterization of hydroxyapatite: potentiometric titrations coupled with solubility measurements. J Colloid Interface Sci 2007;308:405.
[29] Rodenas LG, Palacios JM, Apella MC, Morando PJ, Blesa MA. Surface properties of various powdered hydroxyapatites. J Colloid Interface Sci 2005;290:145.
[30] Somasundaran P, Ofori Amankonah J, Ananthapadmabhan KP. Mineral-solution equilibria in sparingly soluble minerals systems. Colloids Surf 1985;15:309.
[31] Hanna HS, Somasundaran P. Flotation of salt-type minerals. In: Fuerstenau MC, editor. Flotation, A.M. Gaudin Memorial, vol. 1. New York: AIME; 1976. p. 197.
[32] Smani MS, Blazy P, Cases JM. Beneficiation of sedimentary moroccan phosphate ores; part I: electrochemical properties of some minerals of the apatite group. Trans SME/AIME 1975;258:168.
[33] Somasundaran P. Zeta potential of apatite in aqueous solutions and its change during equilibration. J Colloid Interface Sci 1968;27:659.
[34] Su T, Chen T, Zhang Y, Hu P. Selective flocculation enhanced magnetic separation of ultrafine disseminated magnetite ores. Minerals 2016;6:86.
[35] Haselhuhnt HJ, Kawatra SK. Effects of water chemistry on hematite selective flocculation and dispersion. Miner Process Extr Metall Rev 2015;36:305.
[36] Beklioglu B, Arol AI. Selective flocculation behaviour of chromite and serpentine. Physicochem Probl Miner Process 2004;38:103.
[37] Eisele TC, Kawatra SK, Ripke SJ. Water chemistry effects in iron ore concentrate agglomeration feed. Miner Process Extr Metall Rev 2005;26:295.